Int J Clin Exp Med 2020;13(11):8544-8552
www.ijcem.com /ISSN:1940-5901/IJCEM0118128

Original Article

Silencing PARP-1 gene improves heart function and reduces cardiomyocyte apoptosis in rats with heart failure after myocardial infarction

Junwei Ge, Bing Jiang, Shihua Tong, Yinghui Xu, Xuan Zhang, Haining Ju

Department of Cardiology, Seventh People's Hospital of Shanghai University of Traditional Chinese Medicine, Shanghai, China

Received July 14, 2020; Accepted August 15, 2020; Epub November 15, 2020; Published November 30, 2020

Abstract: Objective: We aimed to explore the mechanism by which silencing poly (ADP-ribose) polymerase-1 (PARP-1) improveses the heart function and cardiomyocyte proliferation and apoptosis in rat model of heart failure. Methods: The rats were assigned into the following groups: the sham, model (rat model of heart failure), sham+PARP-1 NC (injected with 0.3 mL of phosphate-buffered saline containing recombinant adenovirus with irrelevant sequences), model+PARP-1 NC, and model+PARP-1 siRNA (injected with 0.3 mL of phosphate-buffered saline solution containing recombinant adenovirus expressing small interfering RNA (siRNA) targeting PARP-1). The rats' heart function, levels of PARP-1, Cyclin D1, Bax, and caspase-3, cardiomyocyte viability, and cardiomyocyte apoptosis were examined in each group. Results: Compared with the sham group, the values of left ventricular ejection fraction (LVEF) and fractional shortening, cardiomyocyte viability and the expression levels of Cyclin D1 and Bcl-2 were lower in the model, model+PARP-1 NC, and model+PARP-1 siRNA groups, whereas the expression levels of PARP-1, Bax, and caspase-3, the values of left ventricular posterior wall thickness at end-diastole (LVPWd), interventricular septum thickness at end-diastole (IVSd), left ventricular end-systolic diameter (LVESD), and left ventricular end-diastolic diameter (LVEDD), and the cell apoptosis rate were higher in these groups (all $P<0.05$). Compared with the model group, the values of LVEF and fractional shortening, the cardiomyocyte viability, and the expression levels of Cyclin D1 and Bcl-2 were higher in the model+PARP-1 siRNA group, whereas the expression levels of PARP-1, Bax, and caspase-3, the values of LVPWd, IVSd, LVEDD, and LVESD, and the cell apoptosis rate were lower in this group (all $P<0.05$). Conclusion: Silencing PARP-1 gene can improve cardiomyocyte viability, inhibit cardiomyocyte apoptosis, and improve heart function in rats with heart failure.

Keywords: Cardiovascular disease, cardiomyocyte viability, DNA repairing enzyme, cell apoptosis rate, heart function, cardiomyocyte apoptosis

Introduction

Cardiovascular disease is a life-threatening disease and has become a major health issue in China. The proportion of deaths caused by heart failure due to ventricular remodeling has been rising in patients with cardiovascular disease [1, 2]. One of the major symptoms in patients with heart failure is dysfunction in heart systole and diastole [3]. Loss of a large number of cardiomyocytes and decreased cardiomyocyte contractility are considered to be the primary reasons for the deterioration of left ventricular function in these patients [4, 5]. Therefore, investigating the changes of cardiomyocyte is essential in the study on the heart function of patients with heart failure.

Poly (ADP-ribose) polymerase-1 (PARP-1), existing mainly in eukaryotic cells, is a proteinase that can catalyze poly ADP-ribosylation in human body [6]. This enzyme participates in DNA repair, gene integrity maintenance, and cell apoptosis regulation within a cell [7-9]. Many studies have demonstrated that PARP-1 plays a critical role in the pathogenesis of cancer [10]. In recent years, many researchers have reported that aberrant expression of PARP-1 is also closely associated with cardiovascular diseases [11]. It has been shown that

Table 1. Sequence silencing

siRNA	Target sequence
siRNA PARP-1	GGTACCATCCAACTTGCTT
Ad-CMV-EGFP	TTTATAGAGGTTGTACTCC

Note: PARP-1: poly (ADP-ribose) polymerase-1; siRNA: small interfering RNA.

increased expression of PARP-1 promotes cardiomyocyte apoptosis during the onset of heart failure in mice [12]. In addition, in a study by Pacher et al., it was found that the expression level of PARP-1 increases significantly in congenital heart disease, heart failure, and arrhythmia [13]. Also, some studies have documented that the loss of PARP-1 is of great significance to the improvement of heart function in patients with Chagas disease [14]. These findings indicate that PARP1 is involved in the pathogenesis of cardiovascular diseases including heart failure. Moreover, PARP-1 overactivation has been found in neurodegenerative diseases such as Parkinson's disease and Alzheimer's as well as in diseases related to oxidative stress and mitochondrial dysfunction such as acute cerebral ischemia and cerebral ischemia-reperfusion [15]. However, the mechanism regarding how this gene affects cardiovascular diseases and patients' heart function remains unclear. Therefore, our study aimed to investigate the impacts of PARP-1 gene on the cardiomyocyte proliferation and apoptosis as well as heart function in the rat model of heart failure, in an effort to find the potential treatment target for patients with heart failure.

Materials and methods

Study subjects and model creation

Fifty-five male Wistar rats at one week of age were chosen for this study (supplier: Better Biotechnology Co., Ltd., Nanjing, China). The conditions for raising the rats met the standards for care and use of experimental animals in medical research. The room temperature was set at 22±2°C, and relative humidity was set at 60±2%. The rats did not undergo fasting before the operation. They were fed with standard granular feed and had ad libitum access to food and water. The circadian cycle was 12 hours. Twenty rats were randomly picked out of the 55 rats and assigned to the sham group, while the rest 35 rats were used for the establishment of the disease model. The mouse model of heart failure following myocardial infarction was constructed by ligating the left coronary artery at the lower edge of left atrial appendage in rats. In the sham group, the rats were only treated with threading without ligation. Echocardiography was conducted on the rats with a cardiac ultrasound device (SonoAce X8, Shanghai Jumu, China) in the fourth week after operation. The model of heart failure was considered to be successfully established, if the value of left ventricular ejection fraction (LVEF) was no more than 45% [16]. All the animal experiments in our study complied with the Declaration of Helsinki and the ARRIVE guidelines and was carried out in accordance with the National Institutes of Health guide for the care and use of laboratory animals (NIH Publications No. 8023, revised 1978). The work was approved by the Institutional Animal Care and Use Committee of Seventh People's Hospital of Shanghai University of Traditional Chinese Medicine.

Since there were limitations to the research conditions and the use of both males and females for the animal experiment can increase the cost and may cause deviations, only one sex was used in our study. However, we will include sex factor in the future experiments for improvement.

Production of recombinant adenovirus (rAdv)

According to the PARP-1 mRNA sequence in the nucleotide database of the National Center for Biotechnology Information, the small interfering RNA (siRNA) sequence targeting PARP-1 gene was designed, and the adenoviral vector siRNA PARP-1 and empty adenoviral vector Ad-CMV-eGFP were constructed. Plasmid pLenR-GPH (Engreen Biosystem Co., Ltd., China) was used as a vector for producing adenoviral vector siRNA PARP-1 targeting PARP1 gene, adenoviral vector OE-PARP-1 overpexressing PARP-1, and empty adenoviral vector Ad-CMV-eGFP. Double-stranded DNA oligonucleotides containing interference sequences were synthesized and directly linked to the enzyme-digested vector. See **Table 1**.

Grouping

The rats in the control group were divided into two subgroups of ten rats each: the sham group (the rats were injected with 0.3 mL of normal saline through tail vein) and the

Table 2. qRT-PCR primer sequence

Gene	Sequence
PARP-1	Forward: 5'-ACGCACAATGCCTATGAC-3'
	Reverse: 5'-CCAGCGGAACCTCTACAC-3'
Cyclin D1	Forward: 5'-TGGAGCCCCTGAAGAAGAG-3'
	Reverse: 5'-AAGTGCGTTGTGCGGTAGC-3'
Bax	Forward: 5'-GGTTTCATCCAGGATCGAGCA-3'
	Reverse: 5'-CGTCAGCAATCATCCTCTGCA-3'
Bcl-2	Forward: 5'-GCCTCCTCACCTTTCAGCAT-3'
	Reverse: 5'-CACTCGTAGCCCTCTGTGAC-3'
caspase-3	Forward: 5'-GCACTGGAATGTCAGCTCGCAA-3'
	Reverse: 5'-GCCACCTTCCGGTTAACACGAC-3'
GAPDH	Forward: 5'-GGCAAGTTCAATGGCACAGT-3'
	Reverse: 5'-TGGTGAAGACGCCAGTAGACTC-3'

Note: PARP-1: poly (ADP-ribose) polymerase-1.

sham+PARP-1 NC group (the rats were injected through tail vein with 0.3 mL of phosphate-buffered saline (PBS) containing rAdv with irrelevant sequences).

The rats with heart failure were divided into three subgroups of ten rats each: the model group (untreated), the model+PARP-1 siRNA group (the rats were injected through tail vein with 0.3 mL PBS solution containing rAdv expressing siRNA targeting PARP-1), and the model+PARP-1 NC group (the rats were injected through tail vein with 0.3 mL PBS solution containing rAdv with irrelevant sequences). The heart function of the rats in the first, second, and fourth week after treatment was measured by echocardiography in each group. Afterward, the rats underwent fasting for 12 h followed by intraperitoneal injection of 2% pentobarbital sodium (50 mg/kg) for anesthesia. The blood samples were taken from the heart and placed in serum tubes. Some myocardial tissues were collected from the modeled rats and kept at -80°C, while the remaining myocardial tissues were fixed with 10% neutral formalin, dehydrated through a gradient of alcohol after 24 h, and were kept at -20°C.

Echocardiography

Echocardiography was performed for detecting the heart function in the rats in the first, second, and fourth week after treatment [17]. The rats in each group received intraperitoneal injection of 2% pentobarbital sodium (50 mg/kg) for anesthesia. After shaving chest hair, the rats were fixed on a piece of wooden board in a supine position. Levels of left ventricular posterior wall thickness at end-diastole (LVPWd), interventricular septum thickness at end-diastole (IVSd), left ventricular end-diastolic diameter (LVEDD), LVEF, left ventricular end-systolic diameter (LVESD), and fractional shortening (FS) were measured with a color ultrasonic device (SSI-5000, Shandong Shukang Hengtong, China).

qRT-PCR

Myocardial tissues (30 mg) were taken from the rats in each group, treated with 1 mL Trizol (Invitrogen, USA), and comminuted in an ice bath. Total RNA extraction was carried out according to the Trizol's instruction manual. Reverse transcription of RNAs into cDNAs (50 ng/μL) was conducted using PrimeScript™ RT reagent kit (Takara, RR047A, Beijing ThinkFar, China). The total reaction volume was 10 μL, and the conditions were as follows: 37°C for 45 min and 85°C for 5 s. The samples were kept at -80°C. The primers were designed by Premier 5.0 software and were synthesized by Tsingke Biological Technology (Beijing, China). The two-step method was conducted with the ABI 7900HT real-time PCR system (ABI 7900, Shanghai Pudi Biotech, China). GAPDH I (abs830032, Absin Bioscience Inc., China) was used as the internal control and the running parameters of PCR were as follows: 95°C for 30 s (pre-denaturation), 95°C for 5 s (denaturation), 58°C for 30 s (annealing), and 72°C for 15 s (extension) for 40 cycles. See **Table 2**.

Western blot

Myocardial tissues (30 mg) were taken from the rats in each group and ground into fine homogeneous powder at a low temperature. After washing in PBS three times, the samples were treated with protein lysis buffer and placed on ice for 20 min, before being centrifuged at 12,000 rpm for 20 min. The supernatant was then collected for measuring the total protein concentration using the BCA protein assay kit (P0012-1, Beyotime, China). Protein (50 μg) was dissolved in 2× SDS sample loading buffer and were boiled at 100°C for 5 min. Afterward, the samples were separated by 10% SDS-PAGE and transferred to polyvinylidene fluoride membrane. The membrane was blocked in 5% skim milk solution for 1 h at room temperature and washed in PBS twice. Next, the polyvinylidene fluoride membrane was incu-

bated with rabbit anti-mouse primary antibodies, which were anti-PARP-1 antibody (9532s, Cell Signaling Technology, Inc., USA), anti-Cyclin D1 antibody (ab40754, Abcam, UK), anti-Bax antibody (ab32503, Abcam, UK), anti-Bcl-2 antibody (ab692, Abcam, UK), and anti-caspase-3 antibody (ab90437, Abcam, UK) with dilutions of 1:1,000, followed by wash in TBST three times (5 min per wash). Subsequently, the membrane was incubated with HRP-conjugated secondary antibody IgG (goat anti-rabbit, ab20272, Abcam, UK) for one hour followed by wash in TBST three times (5 min per wash). Afterward, the samples were treated with ECL, and the image was captured on an x-ray film and photographed. The absorbance value for the visualized band was analyzed with a gel imaging system (Image J 2.0, Thermo Fisher Scientific, USA).

Separation and culture of cardiomyocyte

The rats' myocardial tissues from each group were cut into small cubes (1 mm^3) using an eye scissor under aseptic condition. The samples were added with 3 mL 0.2% collagenase, type II (Sigma-Aldrich, USA) and were bathed in water at 37°C for 6 min. Next, the samples were digested with 3 mL 0.25% pancreatin (Sigma-Aldrich, USA) in a water bath for 5 min. After gently pipetting up and down, the supernatant was obtained and placed in 3 mL of DMEM containing 10% fetal bovine serum. The culture solution was then filtered using a 200-mesh strainer. The filtered solution was centrifuged at 2,000 rpm for 10 min. Subsequently, the cells were collected and added with serum-free DMEM for preparing cell suspensions.

MTT

The cell suspension from each group was seeded onto a 96-well plate (100 μL per well), with 8 replicate wells for each group. The plates were placed in a 5% CO_2 cell culture incubator at 37°C and were taken out at 24, 48, and 72 h for the addition of 10 μL 5 mg/mL MTT solution (Sigma-Aldrich, USA) followed by another 4-hour incubation. Afterward, the supernatant was discarded, and 150 μL dimethyl sulfoxide was dispensed into each well. The samples were then agitated for 10 min for dissolving, and the OD value at 490 nm in each well was measured with an automated microplate reader (BIO-RAD, USA). The experiments were done in triplicate for each group to calculate the average value. Cell viability curves were plotted using time on the x-axis and OD value on the y-axis.

Flow cytometry

The cell suspension in each group was treated with pancreatin without EDTA, and the cells were collected in FACS tubes. After centrifugation, the supernatant was discarded, and the cells were washed in cold PBS for three times. The samples were centrifuged again, and the supernatant was discarded. According to the instructions of Annexin-V-fluorescein isothiocyanate (FITC) apoptosis detection kit (C1065, Beyotime, China), Annexin-V-FITC/propidium iodide (PI) dye was prepared using Annexin-V-FITC, PI, and HEPES buffer (1:2:50). The cells ($1 * 10^6$) were resuspended with 100 μL of dye, and the solution was agitated and mixed. Subsequently, the cells were incubated for 15 min at room temperature and were added with 1 mL of HEPES buffer followed by agitation and mixing. Fluorochrome was excited at 488 nm, and the FITC and PI fluorescence were detected using bandpass filters (525 nm and 620 nm). Cell apoptosis was then measured with a flow cytometry (Beckman Coulter, USA). Apoptosis rate was calculated as the number of apoptotic cell/total cell count * 100%.

Statistical analysis

Statistical software SPSS 21.0 was applied for data analysis. Measurement data are expressed as mean ± standard deviation, and comparisons between two groups were performed by t-test. Comparisons between multiple groups were performed by one-way analysis of variance, and subsequent comparisons between two groups were conducted using the SNK method. $P<0.05$ was considered to indicate a statistically significant difference.

Results

Model establishment

Three rats died during model construction due to severe heart failure and hepatic ascites; another two rats received anesthesia and exsanguination for euthanasia as their LVEF levels did not meet the model criteria. Therefore, the disease model was successfully constructed in 30 rats (success rate of model establishment: 85.71%). The rats with heart failure exhibited symptoms including loss of

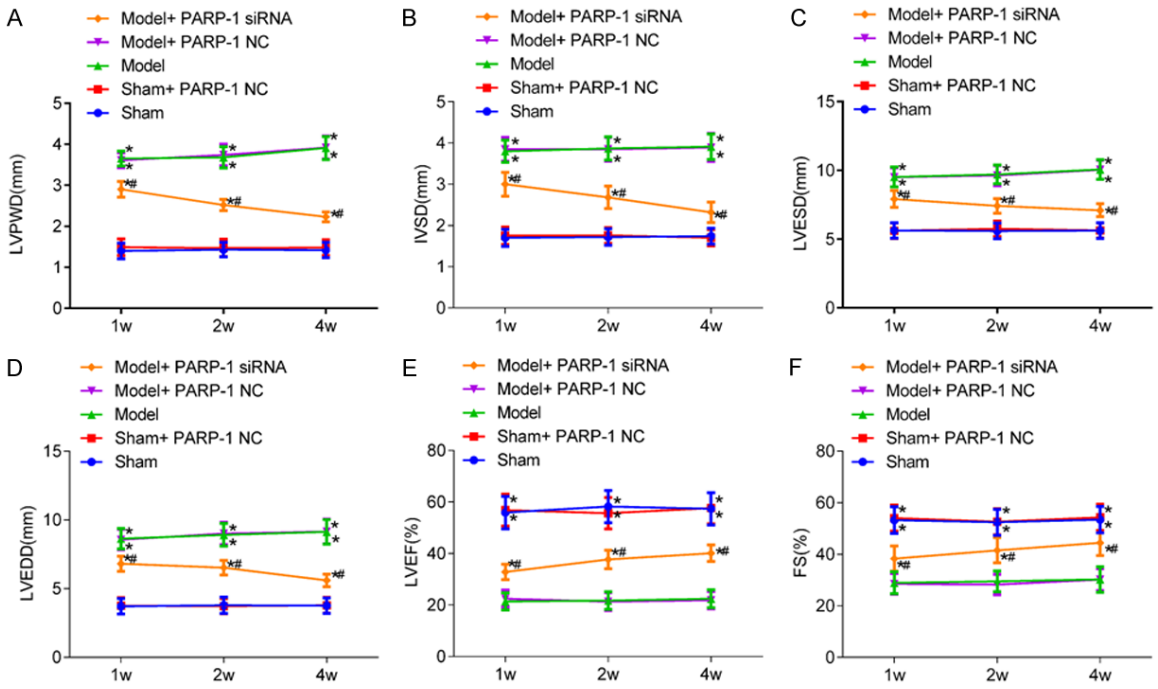

Figure 1. Echocardiography results in each group. A: Histogram of LVPWd results in each group; B: Histogram of IVSD results in each group; C: Histogram of LVESD results in each group; D: Histogram of LVEDD results in each group; E: Histogram of LVEF results in each group; F: Histogram of FS results in each group. *P<0.05 vs. the sham group; #P<0.05 vs. the model group. FS: fractional shortening; IVSd: interventricular septum thickness at end-diastole; LVEDD: left ventricular end-diastolic diameter; LVESD: left ventricular end-systolic diameter; LVEF: left ventricular ejection fraction; LVPWd: left ventricular posterior wall thickness at end-diastole.

appetite, lethargy, mouth breathing, and fatigue.

Echocardiography results in each group

As shown in **Figure 1**, the model, model+PARP-1 NC, and model+PARP-1 siRNA groups had higher levels of LVPWd, IVSd, LVEDD, and LVESD, and lower levels of LVEF and FS compared with the sham group (all P<0.05). Meanwhile, the model PARP-1 siRNA group had lower levels of LVPWd, IVSd, LVEDD, and LVESD, and higher levels of LVEF and FS than the model group (all P<0.05). No intergroup differences in these markers were observed between the sham group and the sham+PARP-1 NC group and between the model group and the model+PARP-1 NC group (all P>0.05).

mRNA and protein expression levels of PARP-1, Cyclin D1, Bax, Bc1-2, and caspase-3 in myocardial tissues in each group

The results of qRT-PCR and western blot showed that in comparison with the sham group, the mRNA and protein expression levels of Cyclin D1 and Bc1-2 were downregulated in the model, model+PARP-1 NC, and model+PARP-1 siRNA groups, while the PARP-1, Bax, and caspase-3 mRNA and protein expression levels were upregulated in these groups (all P<0.05). In comparison with the model group, the mRNA and protein expression levels of Cyclin D1 and Bc1-2 were upregulated, whereas the mRNA and protein expression levels of PARP-1, Bax, and caspase-3 were downregulated in the model+PARP-1 siRNA group (all P<0.05). No differences were found between the sham+PARP-1 NC group and the sham group and between the model group and the model+PARP-1 NC group in the expression levels of these markers (all P>0.05). See **Figure 2**.

Cardiomyocyte viability

The results of cardiomyocyte viability measured by MTT displayed that compared with the sham group, the cardiomyocyte viability was lower at all time points in the model, model+PARP-1 NC, and model+PARP-1 siRNA groups (all P<0.05). Meanwhile, the model+PARP-1 siRNA group had greater cardiomyocyte viability at all time points than the model group (all P<0.05). There

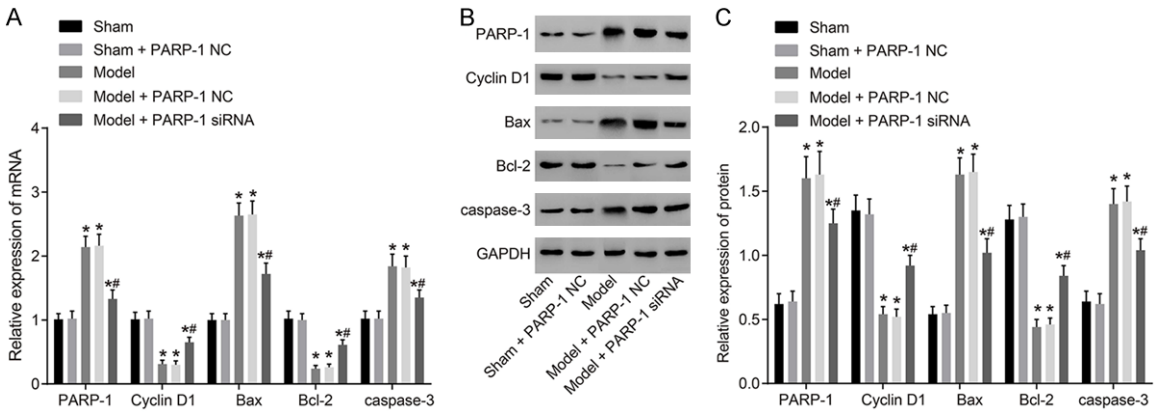

Figure 2. mRNA and protein expression levels of PARP-1, Cyclin D1, Bax, Bcl-2, and caspase-3 in myocardial tissues in each group measured by qRT-PCR and western blot. A: mRNA expression levels of PARP-1, Cyclin D1, Bax, Bcl-2, and caspase-3 in each group detected by qRT-PCR; B: Protein electrophoresis results in each group detected by western blot; C: Protein expression levels of PARP-1, Cyclin D1, Bax, Bcl-2, and caspase-3 in each group detected by western blot. *P<0.05 vs. the sham group; #P<0.05 vs. the model group. PARP-1: poly (ADP-ribose) polymerase-1.

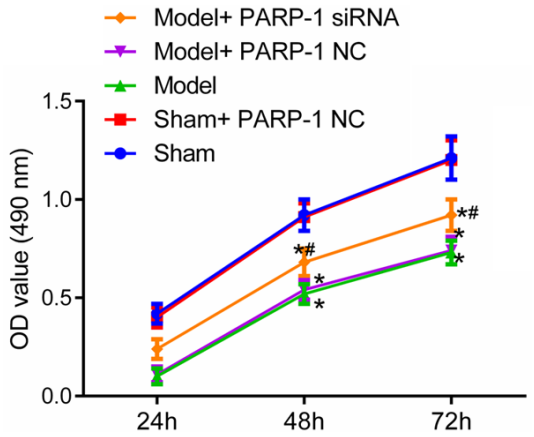

Figure 3. Cardiomyocyte growth at 24, 48, and 72 h in each group. *P<0.05 vs. the sham group; #P<0.05 vs. the model group. OD: optical density.

were no intergroup differences between the sham+PARP-1 NC and the sham group and between the model group and the model+PARP-1 NC group regarding the cardiomyocyte viability at different time points (all P>0.05). See **Figure 3**.

Cardiomyocyte apoptosis in each group

The results of cardiomyocyte apoptosis measured by flow cytometry revealed that compared with the sham group, the cardiomyocyte apoptosis rate was higher in the model, model+PARP-1 NC, and model+PARP-1 siRNA groups (all P<0.05). Meanwhile, the model+PARP-1 siRNA group had a lower cardiomyocyte apoptosis rate than the model group (all P<0.05). No intergroup differences were observed between the sham+PARP-1 NC and the sham group and between the model group and the model+PARP-1 NC group in the apoptosis rate (all P>0.05). See **Figure 4**.

Discussion

PARP-1, as one of the DNA repair enzymes, serves a key role in regulating cellular apoptosis and proliferation [18, 19]. The expression of PARP-1 is low under normal condition, however, in recent years, it has been found that the expression of this gene is noticeably activated in cardiovascular diseases such as atherosclerosis, cerebral stroke, and cerebral ischemia [20, 21]. In this study, we used rAdv to mediate PARP-1 expression and investigated the impacts of this gene on heart function and cardiomyocyte in rats with heart failure. The results have demonstrated that PARP-1 gene silencing can promote cardiomyocyte proliferation, inhibit cardiomyocyte apoptosis, and exhibit marked protective effects on rats' heart function in rats with heart failure.

Apoptosis refers to a form of programmed cell death, and cardiomyocyte apoptosis plays a critical role in regulating cardiac structure and function [22, 23]. A marked decrease in cardiomyocytes can damage the intercalated disc of these cells. Excessive cardiomyocyte apoptosis can cause increased pressure in the heart chamber, thinning of the infarct site, and prolonged cellular apoptosis in non-infarcted zone, which can lead to ventricular hypertrophy and

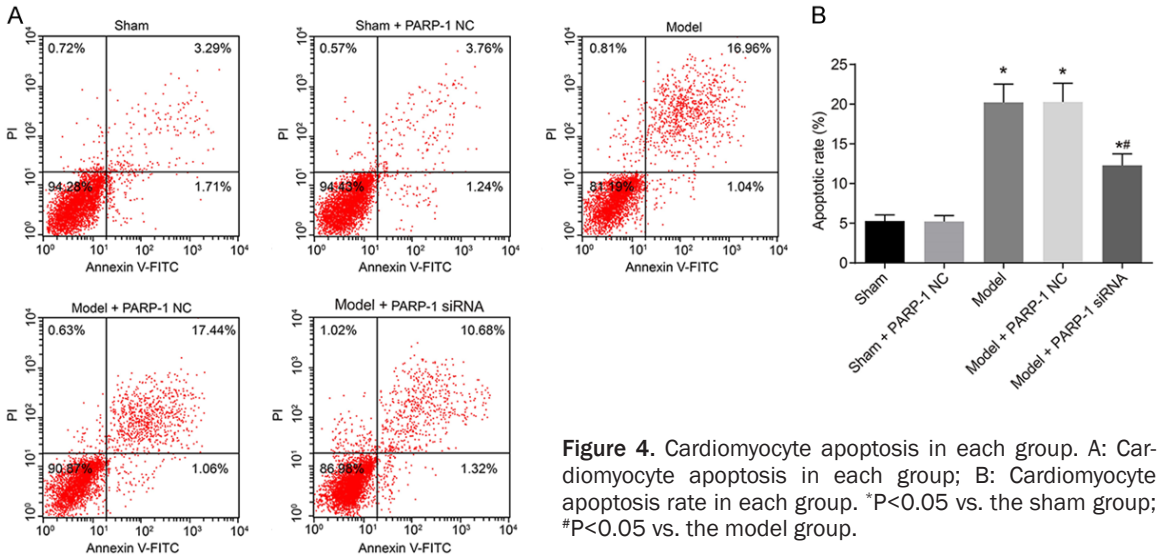

Figure 4. Cardiomyocyte apoptosis in each group. A: Cardiomyocyte apoptosis in each group; B: Cardiomyocyte apoptosis rate in each group. *P<0.05 vs. the sham group; #P<0.05 vs. the model group.

progressive cardiac chamber dilation and worsen the heart function [24-27]. Therefore, it is essential to explore the biological changes in cardiomyocytes in heart failure in order to understand the pathogenesis of this disease and the impact of the biological features of cardiomyocyte on heart function. Lucas et al. reported that inhibiting cardiomyocyte apoptosis in patients with myocardial infarction can reverse the ventricular remodeling and help to improve the heart function [28]. Currently, many studies have demonstrated that overexpression of PARP-1 can significantly damage cardiomyocytes [29, 30]. Zhonghua et al. reported the presence of PARP-1 overactivation in rats with acute ischemia-reperfusion injury, and inactivation of PARP-1 can markedly attenuate myocardial injury and enhance rats' heart function [31]. Korkmaz-Icöz et al. found that PARP-1 gene knockout can reduce cardiomyocyte apoptosis, improve vascular endothelial function, and significantly relieve symptoms in rats with myocardial remodeling [32].

LVPWd and IVSd are two critical markers in evaluating left ventricular hypertrophy, while LVEDD and LVESD are essential markers in assessing left ventricular systolic and diastolic capacity and can have great impacts on LVEF and FS [33]. The results of the present study exhibited that after treatment, the ventricular systolic and diastolic capacity were significantly improved and the ventricular remodeling was remarkably relieved in rats with PARP-1 gene silencing, supporting that the silence of this gene can serve a positive role in the treatment of heart failure. In order to further investigate the detailed mechanism by which PARP-1 affects the heart function in rats with heart failure, we detected cardiomyocyte proliferation and apoptosis in each group. The results showed that the PARP-1 siRNA group had higher expression levels of proteins relating to the cell proliferation, greater cardiomyocyte viability, and lower cardiomyocyte apoptosis rate compared with other groups, indicating that PARP-1 can serve a key role in the pathogenesis of heart failure and suppressing PARP-1 expression can be of great significance in promoting cardiomyocyte proliferation.

Although the effect of PARP-1 gene silencing on heart failure was explored in this study, the detailed mechanism regarding how PARP-1 regulates heart failure remains unclear. Therefore, more studies need to be conducted in the future for verification.

In conclusion, PARP-1 gene silencing can significantly promote cardiomyocyte proliferation, inhibit cardiomyocyte apoptosis, and display protective effects on rats' heart function in rats with heart failure. As a result, PARP-1 can be a potential key target for treating heart failure.

Acknowledgements

This work was supported by The Outstanding Clinical Discipline Project of Shanghai Pudong New Area (PWYgy2018-05).

Disclosure of conflict of interest

None.

Address correspondence to: Haining Ju, Department of Cardiology, Seventh People's Hospital of Shanghai University of Traditional Chinese Medicine, No. 358 Datong Road, Pudong New Area, Shanghai 200137, China. Tel: +86-021-58670561-6330; E-mail: juhaininguy3e@163.com

References

[1] Jorsal A, Kistorp C, Holmager P, Tougaard RS, Nielsen R, Hanselmann A, Nilsson B, Møller JE, Hjort J, Rasmussen J, Boesgaard TW, Schou M, Videbæk L, Gustafsson I, Flyvbjerg A, Wiggers H and Tarnow L. Effect of liraglutide, a glucagon-like peptide-1 analogue, on left ventricular function in stable chronic heart failure patients with and without diabetes (LIVE)-a multicentre, double-blind, randomised, placebo-controlled trial. Eur J Heart Fail 2017; 19: 69-77.

[2] Lottonen-Raikaslehto L, Rissanen R, Gurzeler E, Merentie M, Huusko J, Schneider JE, Liimatainen T and Ylä-Herttuala S. Left ventricular remodeling leads to heart failure in mice with cardiac-specific overexpression of VEGF-B167: echocardiography and magnetic resonance imaging study. Physiol Rep 2017; 5: e13096.

[3] Chirinos JA, Akers SR, Trieu L, Ischiropoulos H, Doulias PT, Tariq A, Vasim I, Koppula MR, Syed AA, Soto-Calderon H, Townsend RR, Cappola TP, Margulies KB and Zamani P. Heart failure, left ventricular remodeling, and circulating nitric oxide metabolites. J Am Heart Assoc 2016; 5: e004133.

[4] Ghosh AK, Rai R, Flevaris P and Vaughan DE. Epigenetics in reactive and reparative cardiac fibrogenesis: the promise of epigenetic therapy. J Cell Physiol 2017; 232: 1941-1956.

[5] Gyongyosi M, Haller PM, Blake DJ and Martin Rendon E. Meta-analysis of cell therapy studies in heart failure and acute myocardial infarction. Circ Res 2018; 123: 301-308.

[6] Bhat KR, Benton BJ, Rosenthal DS, Smulson ME and Ray R. Role of poly(ADP-ribose) polymerase (PARP) in DNA repair in sulfur mustard-exposed normal human epidermal keratinocytes (NHEK). J Appl Toxicol 2000; 20 Suppl 1: S13-7.

[7] Zhao H, Zhang J and Hong G. Minocycline improves cardiac function after myocardial infarction in rats by inhibiting activation of PARP-1. Bilmed Pharmacother 2018; 97: 1119-1124.

[8] Weaver AN, Cooper TS, Rodriguez M, Trummell HQ, Bonner JA, Rosenthal EL and Yang ES. DNA double strand break repair defect and sensitivity to poly ADP-ribose polymerase (PARP) inhibition in human papillomavirus 16-positive head and neck squamous cell carcinoma. Oncotarget 2015; 6: 26995-27007.

[9] Yao H, Ji M, Zhu Z, Zhou J, Cao R, Chen X and Xu B. Discovery of 1-substituted benzyl-quinazoline-2,4(1H,3H)-dione derivatives as novel poly(ADP-ribose)polymerase-1 inhibitors. Bioorg Med Chem 2015; 23: 681-693.

[10] Mangia A, Scarpi E, Partipilo G, Schirosi L, Opinto G, Giotta F and Simone G. NHERF1 together with PARP1 and BRCA1 expression as a new potential biomarker to stratify breast cancer patients. Oncotarget 2017; 8: 65730-65742.

[11] Wen JJ, Yin YW and Garg NJ. PARP1 depletion improves mitochondrial and heart function in Chagas disease: effects on POLG dependent mtDNA maintenance. PLoS Pathog 2018; 14: e1007065.

[12] Pillai JB, Russell HM, Raman J, Jeevanandam V and Gupta MP. Increased expression of poly(ADP-ribose) polymerase-1 contributes to caspase-independent myocyte cell death during heart failure. Am J Physiol Heart Circ Physiol 2005; 288: H486-496.

[13] Pacher P and Szabo C. Role of poly(ADP-ribose) polymerase 1 (PARP-1) in cardiovascular diseases: the therapeutic potential of PARP inhibitors. Cardiovasc Drug Rev 2007; 25: 235-260.

[14] Garg NJ, Soman KV, Zago MP, Koo SJ, Spratt H, Stafford S, Blell ZN, Gupta S, Burgos JN, Barrientos N, Brasier AR and Wiktorowicz JE. Changes in proteome profile of peripheral blood mononuclear cells in chronic chagas disease. PLoS Negl Trop Dis 2016; 10: e0004490.

[15] Narne P, Pandey V, Simhadri PK and Phanithi PB. Poly (ADP-ribose) polymerase-1 hyperactivation in neurodegenerative diseases: the death knell tolls for neurons. Semin Cell Dev Biol 2017; 63: 154-166.

[16] Smiley D, Smith MA, Carreira V, Jiang M, Koch SE, Kelley M, Rubinstein J, Jones WK and Tranter M. Increased fibrosis and progression to heart failure in MRL mice following ischemia/reperfusion injury. Cardiovasc Pathol 2014; 23: 327-334.

[17] Khan M, Nickoloff E, Abramova T, Johnson J, Verma SK, Krishnamurthy P, Mackie AR, Vaughan E, Garikipati VN, Benedict C, Ramirez V, Lambers E, Ito A, Gao E, Misener S, Luongo T, Elrod J, Qin G, Houser SR, Koch WJ and Kishore R. Embryonic stem cell-derived exosomes promote endogenous repair mechanisms and enhance cardiac function following myocardial infarction. Circ Res 2015; 117: 52-64.

[18] Yan S, Liu L, Ren F, Gao Q, Xu S, Hou B, Wang Y, Jiang X and Che Y. Sunitinib induces genomic instability of renal carcinoma cells through affecting the interaction of LC3-II and PARP-1. Cell Death Dis 2017; 8: e2988.

[19] Luo H, Liang H, Chen Y, Chen S, Xu Y, Xu L, Liu J , Zhou K, Peng J, Guo G, Lai B, Song L, Yang H, Liu L, Peng J, Liu Z, Tang L, Chen W and Tang H. miR-7-5p overexpression suppresses cell proliferation and promotes apoptosis through inhibiting the ability of DNA damage repair of PARP-1 and BRCA1 in TK6 cells exposed to hydroquinone. Chem Biol Interact 2018; 283: 84-90.

[20] Zhang R, Tang S, Huang W, Liu X, Li G, Chi H, Zhu M and Tang J. Protection of the brain following cerebral ischemia through the attenuation of PARP-1-induced neurovascular unit damage in rats. Brain Res 2015; 1624: 9-18.

[21] Hashemi-Niasari F, Rabbani-Chadegani A, Razmi M and Fallah S. Synergy of theophylline reduces necrotic effect of berberine, induces cell cycle arrest and PARP, HMGB1, Bcl-2 family mediated apoptosis in MDA-MB-231 breast cancer cells. Bilmed Pharmacother 2018; 106: 858-867.

[22] Yu S, Wang X, Geng P, Tang X, Xiang L, Lu X, Li J, Ruan Z, Chen J, Xie G, Wang Z, Ou J, Peng Y, Luo X, Zhang X, Dong Y, Pang X, Miao H, Chen H and Liang H. Melatonin regulates PARP1 to control the senescence-associated secretory phenotype (SASP) in human fetal lung fibroblast cells. J Pineal Res 2017; 63.

[23] Li X, Wang H, Yao B, Xu W, Chen J and Zhou X. lncRNA H19/miR-675 axis regulates cardiomyocyte apoptosis by targeting VDAC1 in diabetic cardiomyopathy. Sci Rep 2016; 6: 36340.

[24] Gao CK, Liu H, Cui CJ, Liang ZG, Yao H and Tian Y. Roles of MicroRNA-195 in cardiomyocyte apoptosis induced by myocardial ischemia-reperfusion injury. J Genet 2016; 95: 99-108.

[25] Matyas C, Nemeth BT, Olah A, Torok M, Ruppert M, Kellermayer D, Barta BA, Szabó G, Kökény G, Horváth EM, Bódi B, Papp Z, Merkely B and Tamás Radovits. Prevention of the development of heart failure with preserved ejection fraction by the phosphodiesterase-5A inhibitor vardenafil in rats with type 2 diabetes. Eur J Herat Fail 2017; 19: 326-336.

[26] Moreno MU, Eiros R, Gavira JJ, Gallego C, Gonzalez A, Ravassa S, López B, Beaumont J, José GS and Díez J. The hypertensive myocardium: from microscopic lesions to clinical complications and outcomes. Med Clin North Am 2017; 101: 43-52.

[27] Bao MW, Zhang XJ, Li L, Cai Z, Liu X, Wan N, Hu G, Wan F, Zhang Rui, Zhu X, Xia H and Li H. Cardioprotective role of growth/differentiation factor 1 in post-infarction left ventricular remodelling and dysfunction. J Pathol 2015; 236: 360-372.

[28] Lucas A, Mialet-Perez J, Daviaud D, Parini A, Marber MS and Sicard P. Gadd45gamma regulates cardiomyocyte death and post-myocardial infarction left ventricular remodelling. Cardiovas Res 2015; 108: 254-267.

[29] Gero D, Szoleczky P, Chatzianastasiou A, Papapetropoulos A and Szabo C. Modulation of poly(ADP-ribose) polymerase-1 (PARP-1)-mediated oxidative cell injury by ring finger protein 146 (RNF146) in cardiac myocytes. Mol Med 2014; 20: 313-328.

[30] Tao R, Kim SH, Honbo N, Karliner JS and Alano CC. Minocycline protects cardiac myocytes against simulated ischemia-reperfusion injury by inhibiting poly(ADP-ribose) polymerase-1. J cardiovasc Pharmacol 2010; 56: 659-668.

[31] Zhonghua JI, Zeng L, Cheng Y, Liang G and Anesthesiology DO. Poly(ADP-ribose) polymerases-1 inhibitor MRL-45696 alleviates DNA damage after myocardial ischemia-reperfusion in diabetic rats. Nan Fang Yi Ke Da Xue Xue Bao 2018; 38: 830-835.

[32] Korkmaz-Icöz S, Szczesny B, Marcatti M, Li S, Ruppert M, Lasitschka F, Loganathan S, Szabó C and Szabó G. Olaparib, a clinically used poly(ADP-ribose) polymerase inhibitor protects against oxidant-induced cardiac myocyte death in vitro and improves cardiac contractility during early phase after heart transplantation in a rat model in vivo. Br J Pharmacol 2017; 175: 246.

[33] Seng MC, Shen X, Wang K, Chong DT, Fam JM, Hamid N, Amanullah MR, Yeo KK, Ewe SH, Chua TS, Ding ZP and Sahlén A. Allometric relationships for cardiac size and longitudinal function in healthy chinese adults-normal ranges and clinical correlates. Circ J 2018; 82: 1836-1843.